



Full Length Article

Growth behaviour of low-energy plasma electrolytic oxidation coatings on a magnesium alloy

V. Dehnavi^{a,*}, W.J. Binns^a, J.J. Noël^{a,b}, D.W. Shoesmith^{a,b}, B.L. Luan^{c,a,**}^aDepartment of Chemistry, Western University, London, Ontario N6A 5B7, Canada^bSurface Science Western, Western University, London, Ontario N6G 0J3, Canada^cNational Center for Materials Service Safety, University of Science and Technology Beijing, 30 Xueyuan Road, Haidian District, Beijing 100083, PR China

Received 7 March 2018; received in revised form 29 May 2018; accepted 30 May 2018

Available online 19 June 2018

Abstract

Plasma electrolytic oxidation (PEO), a promising surface treatment method to improve the corrosion and wear resistance of magnesium and its alloys, operates at high voltages, resulting in a relatively high energy cost. To make the PEO process more economically viable, its energy efficiency needs to be improved. This study investigates the growth behaviour and microstructural characteristics of low-energy PEO coatings on an AM50 magnesium alloy in a concentrated electrolyte containing sodium tetraborate. The surface morphology of the coatings was different from typical PEO coating morphologies and a large voltage oscillation was observed during treatment. Using different characterisation techniques, and based on a micro-discharge model, a correlation was made between the voltage-time behaviour, micro-discharge characteristics and the composition and microstructure of the coated samples. The results suggest electrolyte chemistry can somewhat control discharge behaviour, which plays an important role in PEO coating growth.

© 2018 Published by Elsevier B.V. on behalf of Chongqing University.

This is an open access article under the CC BY-NC-ND license. (<http://creativecommons.org/licenses/by-nc-nd/4.0/>)

Peer review under responsibility of Chongqing University

Keywords: Plasma electrolytic oxidation; Magnesium; Oxide coating; Mechanism; Low energy.

1. Introduction

In recent years, magnesium and its alloys have attracted significant interest for applications in the automotive, aerospace, communications and biomedical industries because of their special properties, which include low density, high strength-to-weight ratio, good electromagnetic, noise-reducing and thermal conductivity properties, recycling ability, and superior biocompatibility and biodegradability. However, their application is restricted by poor wear resistance and a susceptibility to corrosion [1–4].

Surface treatment is the general approach adopted to overcome these deficiencies. Several treatments have been devel-

oped, among which plasma electrolytic oxidation (PEO) has proved promising and attracted significant interest recently. During PEO, also known as micro-arc oxidation (MAO), many short-lived micro-discharges are created by dielectric breakdown of the growing oxide film, resulting in the formation of ceramic-like oxide coatings composed of species from both the electrolyte and the sample. These coatings are strongly bonded to the substrate, with good protective properties. An interesting possibility with the PEO process is the incorporation of various types of nano- and micro-sized particles that are added into the electrolyte [5].

PEO operates at high voltages, typically several hundred volts, which results in a relatively high energy cost. For example, the energy cost of PEO coatings on Al alloys can be 20–50 times more than conventional anodizing [6]. For PEO to become more economically viable, its energy efficiency needs to be improved. However, there are few studies exclusively addressing the low-energy formation of PEO coatings. Many factors can influence the PEO process and

* Corresponding author.

** Corresponding author at: National Center for Materials Service Safety, University of Science and Technology Beijing, 30 Xueyuan Road, Haidian District, Beijing 100083, PR China

E-mail addresses: vdehnavi@uwo.ca (V. Dehnavi), bluan@uwo.ca (B.L. Luan).

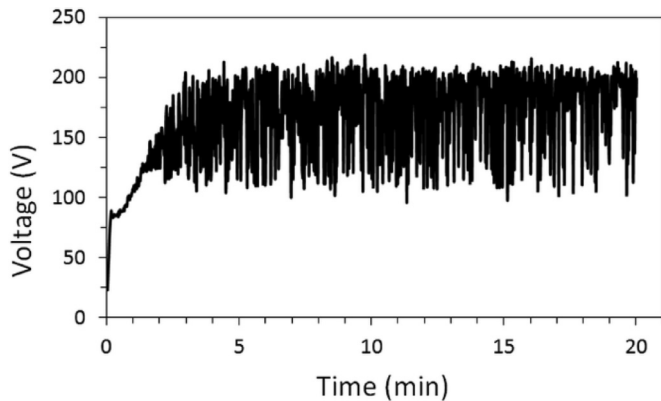


Fig. 1. Voltage-time response during PEO treatment of an AM50 Mg sample at a constant current density of 40 mA/cm².

the properties of the resulting coatings, including the electrical parameters (current density and mode), the electrolyte composition, the substrate material, and the duration of the coating process. Selecting the optimum electrical parameters, modifying the cell geometry design and electrolyte composition, and pre-anodizing to form a precursor oxide prior to PEO are strategies by which the energy consumption of the PEO could be reduced [6,7].

Electrolyte composition plays an important role in the formation of PEO coatings and in determining their properties. Many studies have investigated the effect of electrolyte additives on the properties of the coatings; however, it is difficult to compare the results of these studies, since processing conditions generally differ [8]. The most common electrolytes used for the PEO coating process on Mg alloys are based on potassium and/or sodium hydroxide with additions of phosphates and/or silicates [9–13]. Potassium fluoride [14], sodium fluoride [15,16], and sodium aluminate [8] have also been used. Few studies suggest that the addition of sodium tetraborate can improve the corrosion performance of PEO coatings. Using a concentrated electrolyte solution containing NaOH, Na₂SiO₃, and Na₂B₄O₇, Zhao et al. [17] reported that dense, protective coatings, with a thickness of 30 μm, were obtained on a Mg substrate after 17 min at a relatively low energy cost. Sreekanth et al. [18] reported that the least porosity and best corrosion resistance were obtained using a silicate-based electrolyte solution containing 2 g/L Na₂B₄O₇·10H₂O at a current density of 60 mA/cm². Unfortunately, they did not provide the voltage-time behaviour observed during coating. Ono et al. [19] reported that increasing the concentration of electrolytes containing phosphate, silicate, and aluminate resulted in a decrease in the breakdown and operating voltage of the coating process on the AZ31 Mg alloy.

Despite these endeavours, the influence of the process parameters and electrolyte chemistry on the growth of PEO coatings still needs further investigation, since its effect on the morphology, microstructure, and phase composition of the coatings is complex and inadequately understood [20]. Furthermore, most studies have focused on the influence of electrolyte composition on coating properties, such as

corrosion and wear resistance. The role of electrolyte composition in determining discharge behaviour, which significantly influences the microstructure and morphology of the coatings [21], has received little attention. In this regard, an improved fundamental understanding of the role that electrolyte composition plays in discharge phenomena and how it affects the mechanism of coatings formation is required.

The research presented in this communication is focused on an investigation of the evolution, growth behaviour, and microstructural characteristics of low-energy PEO coatings on a die-cast AM50 Mg alloy in a concentrated electrolyte solution containing sodium tetraborate. The dominant focus is on the correlation between voltage-time behaviour, micro-discharge characteristics and the composition and microstructure of the coatings produced.

2. Material and methods

Specimens of the die-cast AM50 Mg alloy with a nominal chemical composition (wt.%) of 4.5–5.3 Al, 0.28–0.5 Mn, <0.2 Zn, <0.05 Si, <0.008 Cu, <0.001 Ni, <0.004 Fe, and Mg balance, were mounted in epoxy resin and the exposed surface areas ground using emery papers up to P1200 grit. The surface was then degreased in ethanol, rinsed with deionised water and immediately dried with Ar prior to PEO.

PEO was performed in an electrolyte solution containing 20 g/L NaOH, 80 g/L Na₂SiO₃·5H₂O, and 80 g/L Na₂B₄O₇·10H₂O using a direct current power supply. All samples were coated at a constant current density of 40 mA/cm². Samples with an active area of 1 cm², and a rectangular stainless steel wire mesh (3 x 5 cm), were used as the anode and cathode, respectively. The electrolyte was constantly mixed using a magnetic stirrer and its temperature maintained at 22 ± 3 °C during the coating process. Samples were coated for different durations ranging from 1 to 20 min to study the evolution in the properties of the PEO coatings.

The morphology, chemical composition and microstructure of the coatings were analyzed using Hitachi S-4500 field emission and Hitachi SU3500 variable pressure scanning electron microscopes (SEM). Samples were sputtered with gold prior to SEM inspection. Energy dispersive X-ray spectroscopy (EDX) was conducted on a Hitachi SU3500 Variable Pressure SEM in combination with an Oxford Aztec X-Max50 X-ray analyzer. Aztec software allowed for both point analyses as well as the acquisition of EDX maps. Analysis of the phase composition of coatings was performed with an Inel CPS X-ray diffractometer using Cu Kα radiation, in a glancing angle configuration with an incident angle of 4° to minimize interference from the Mg substrate.

3. Results

3.1. Voltage-time response

Fig. 1 shows the voltage-time plot obtained when a constant current density of 40 mA/cm² was applied to an AM50 Mg specimen. The voltage-time plots recorded when coating

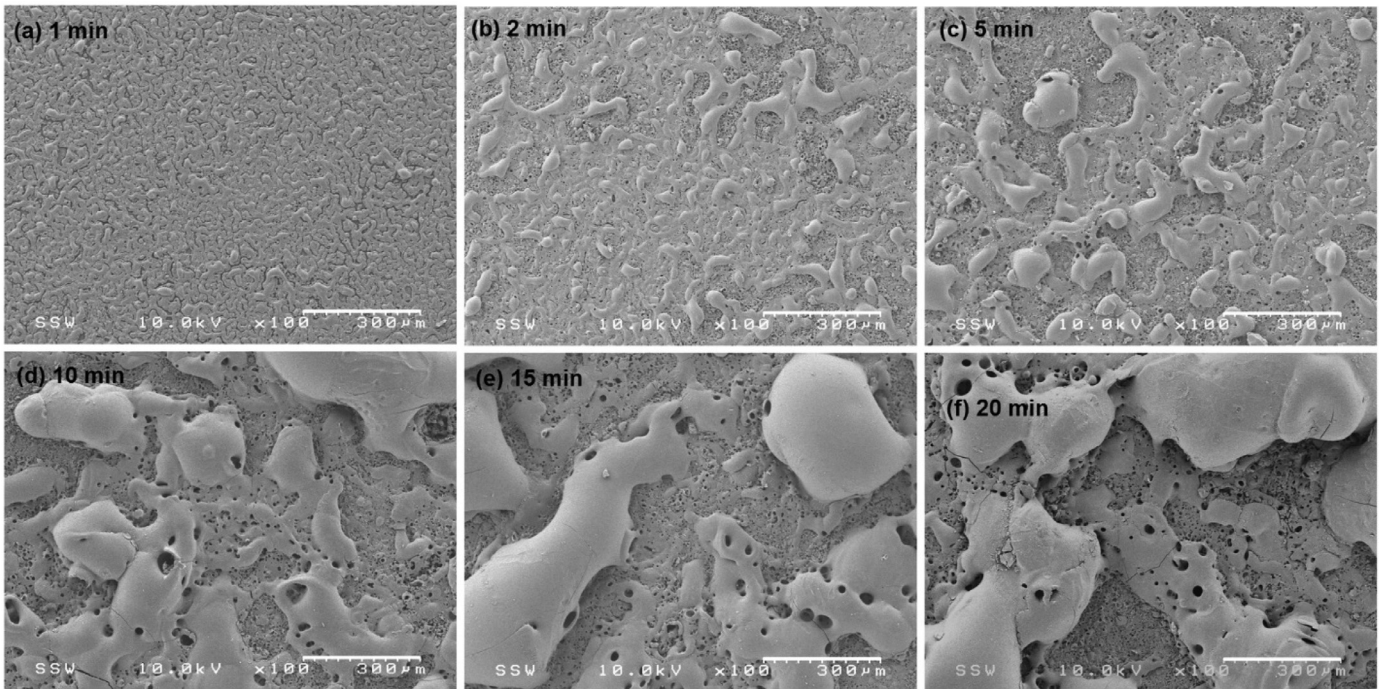


Fig. 2. Surface morphology of PEO coatings on AM50 Mg coated for various durations ranging from 1 to 20 min.

Mg, Al, and Ti alloys typically exhibit an initial abrupt, linear voltage increase, followed by a sudden reduction in the slope. This sudden change in the slope is accompanied by the onset of micro-discharges on the sample surface, and is referred to as the breakdown or sparking voltage. Beyond the breakdown voltage, the voltage typically increases with time at a lower rate until the process is terminated. The value of the breakdown voltage varies depending on the processing conditions and the substrate used. Based on previous literature reports, the breakdown voltage is typically 150–450 V for Mg alloys [4,19,22–24], 300–650 V for Al alloys [25–30], and 200–450 V for Ti alloys [31–35].

The PEO coating in this work was formed at a voltage < 200 V, which is at the lower end of the range of commonly reported voltages for Mg alloys. As can be seen in Fig. 1, a rapid linear increase in voltage occurs over the first few seconds until the breakdown voltage is achieved at ~90 V, when small white sparks become visible on the surface and the rate of voltage increase slows. After ~2 min, the voltage starts to oscillate. At first the amplitude of oscillations is small, but it increases with time. After 3 min, the voltage oscillates between ~100 and 200 V with the range remaining constant thereafter. Such voltage fluctuations have not been commonly reported during PEO, but oscillations between 150 and 350 V were reported in the later stages of PEO by Ono et al. [19] in solutions with a concentration of 82 g/L and 41 g/L Na_3PO_4 . Also, Yagi et al. [36] prepared coatings in two electrolytes, one containing 12 g/L Na_2SiO_3 , the other 82 g/L Na_3PO_4 . The voltage-time plots recorded in both electrolytes exhibited oscillations, with oscillations in the Na_3PO_4 solution similar to those presented here.

3.2. Coating evolution and characterization

Visual observations during PEO showed that the micro-discharges were initially small and white. Their intensity and size increased over time, accompanied by a minor colour change from white to yellow. By contrast to our observations during PEO of Al alloys, when the whole surface was covered with numerous rapidly moving micro-discharges in the early stages [27], in this study micro-discharges had a much lower spatial density.

The changes in the surface morphology and cross-sectional structures of the coatings as a function of treatment time are illustrated in Fig. 2 and Fig. 3, respectively. After 1 min, ~50 s after breakdown, the sample is in the second linear region of the voltage-time plot, Fig. 1. The surface of the sample appears to be partially covered with a layer of PEO coating, Fig. 2-a, with some elongated pores. The cross-section, Fig. 3-a, confirms that the coating is not uniform, with areas of the surface remaining uncoated. After 2 min, elongated pores are not observed, and complete surface coverage appears to have been achieved, Figs. 2-b and 3-b. The time that full coverage is achieved is approximately the time when voltage fluctuations commence, Fig. 1.

Two distinct types of surface feature are distinguishable; globular structures, and a coating matrix with small pores. After 5–20 min, Fig. 2-c to 2-f, the same morphology is observed, but the structure is coarser with larger features. After 20 min of coating, the globular structures reach a few hundred micrometres across. This suggests that micro-discharges become stronger with the duration of processing, with a stronger discharge creating a larger molten mass. Inspection of the

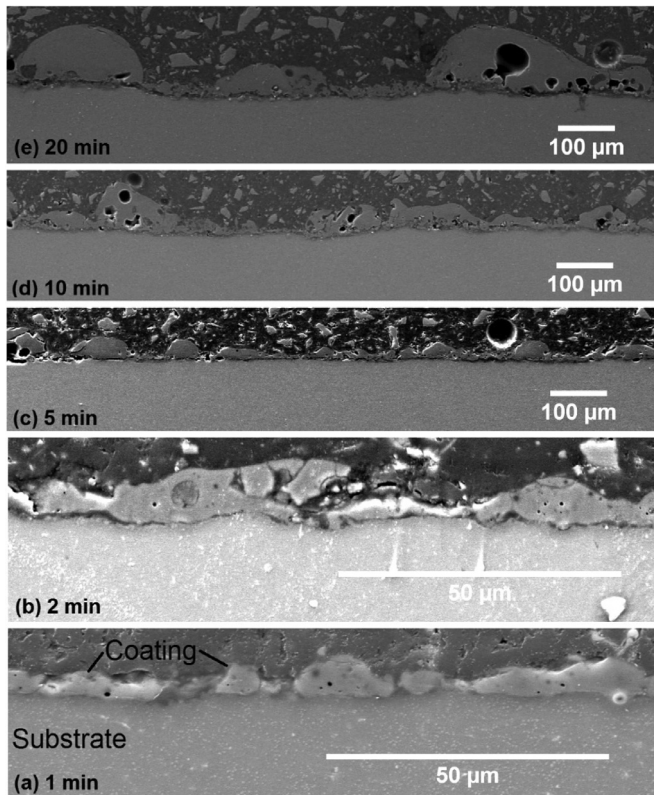


Fig. 3. Cross-sections of PEO coatings formed on AM50 Mg for different durations ranging from 1 to 20 min.

cross-sectional micrographs, Fig. 3, shows that the coating is non-uniform. After 20 min, Fig. 3-f, the coating has a thickness ranging from 20 μm in the matrix to 120 μm in the globular structures.

Hussein et al. [37] investigated the plasma discharge behaviour and coating growth process during PEO treatment of Al in an electrolyte containing Na_2SiO_3 and KOH using optical emission spectroscopy (OES) in the visible and near ultraviolet (NUV) band. They proposed three plasma discharge processes: type A and type C micro-discharges due to gas discharge at the oxide-electrolyte interface, with type A occurring in relatively small holes near the surface, and type C in deeper micro pores, and type B micro-discharges, which are stronger and due to dielectric breakdown, and originate at the metal-oxide interface. The intensity ratio of elements from the substrate (Al) to those from the electrolyte (Si) showed that the concentration of Al was higher in locations associated with type B micro-discharges than at locations associated with types A and C micro-discharges. In type B micro-discharges, film breakdown occurs through the oxide layer down to the Al substrate, enabling the formation of localised melt channels in which plasma reactions occur. As a result, the main source of Al in these locations was from the substrate surface. In types A and C, micro-discharges are less intense, leading to a greater incorporation into the coating of elements from the electrolyte.

The surface morphology of the coatings produced in this study, Fig. 2, is different from that observed for typically ob-

Table 1

Ratios of Mg to Si and Na determined by EDX point analyses on the surface of PEO coatings on AM50 Mg.

Coating duration	Location	Mg/Si	Mg/Na
2 min	Globular	1.3	3.7
	Matrix	1.0	1.9
5 min	Globular	1.3	3.1
	Matrix	1.0	2.2
20 min	Globular	1.1	3.0
	Matrix	1.1	1.7

tained PEO coatings. The usual coating morphology is composed of crater-like features also referred to as “pancake” structures [23,38,39]. The formation of this crater-like morphology with a central hole is attributed to strong type B micro-discharges, which start deep within the coating at the substrate surface. The molten mass produced by a single micro-discharge erupts from the discharge channel and, upon contacting the electrolyte, solidifies rapidly around the discharge channel. This creates the characteristic crater morphology [40]. EDX analyses confirm craters are created by these strong micro-discharges originating at the substrate-coating interface, because the substrate element is dominant in areas immediately adjacent to the crater but becomes less prominent at locations away from the crater [27,41,42].

The distribution of elements in the coatings was determined using EDX mapping and point analyses, Figs. 4 and 5. The cross-sections and EDX elemental maps of samples coated for 1, 10, and 20 min are shown in Fig. 4. These coatings were primarily composed of Mg, O, Si, and Na. Boron, although present in the electrolyte, was not detected, being a light element with a high detection limit. Gold signals are from the sputter coating. Comparisons of elemental maps suggest that the main elements detected are uniformly distributed in the coatings, with no significant differences in distribution observed for different coating times.

SEM micrographs and corresponding EDX spectra from spot analyses are shown in Fig. 5. In samples coated for 2 and 20 min, the globular features and the matrix are primarily composed of Mg, O, Si, and Na, with small amounts of Al, but the elemental distributions are slightly different. Inspection of the EDX spectra in Fig. 5 reveals that, in both samples, Si and Na incorporated from the electrolyte have higher intensities in the matrix (point 2) than in the globular features (point 1).

The elemental ratio on the surface of the coatings can be used to determine the type of micro-discharge occurring during the coating process. Table 1 tabulates the ratios of Mg/Si and Mg/Na for samples coated for different durations, and shows that there is no significant dependence of the elemental distribution on the duration of the coating process. Also noteworthy is that the amount of the substrate material, Mg, is not significantly greater than the amounts of Si and Na, suggesting that micro-discharges occurring during our procedure were of type A and C, and not type B. Based on the Mg/Si and Mg/Na ratios, Table 1, it can be inferred that the

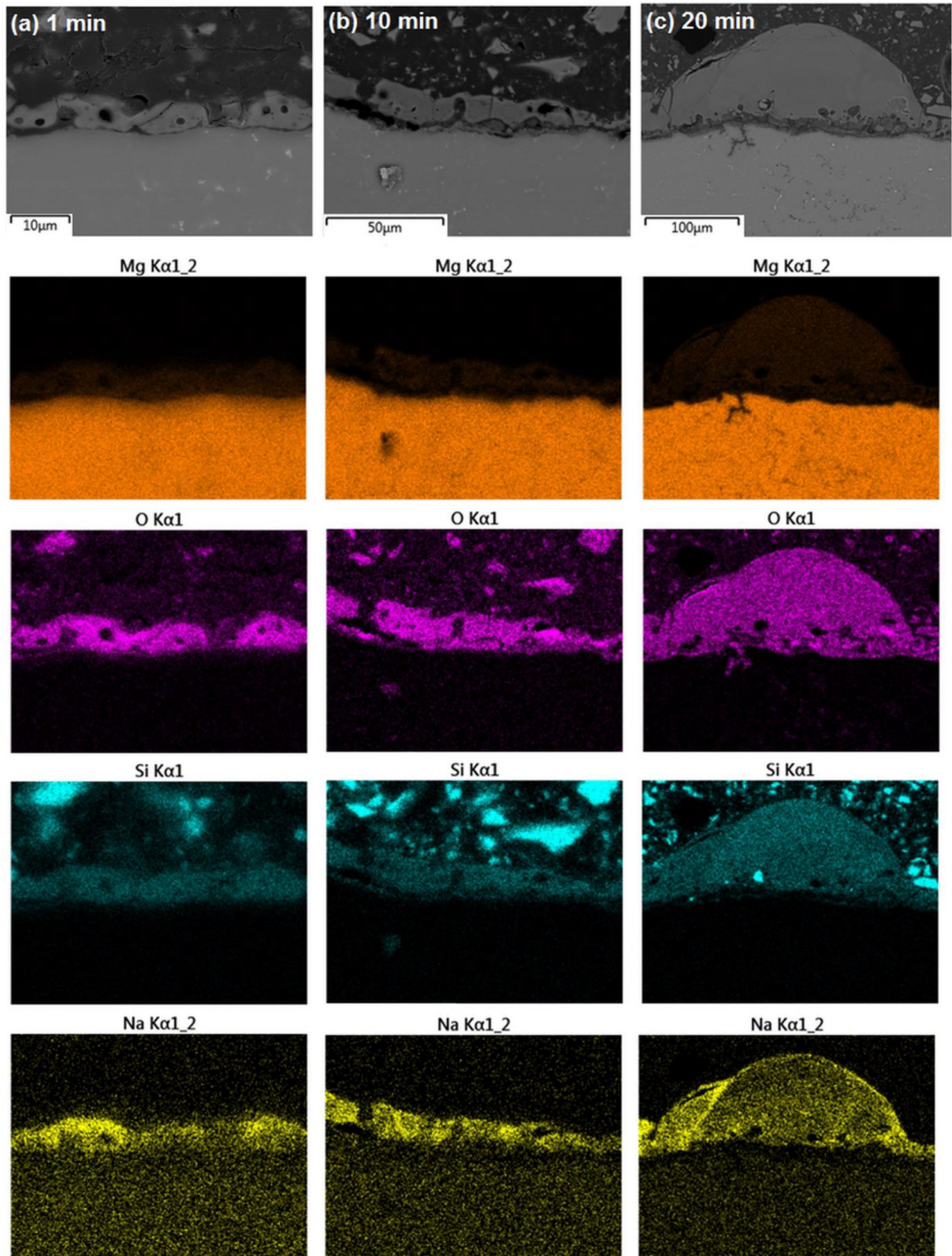


Fig. 4. Backscattered electron images and respective EDX elemental maps of the cross-sections of coatings synthesized for (a) 1 min, (b) 10 min, and (c) 20 min.

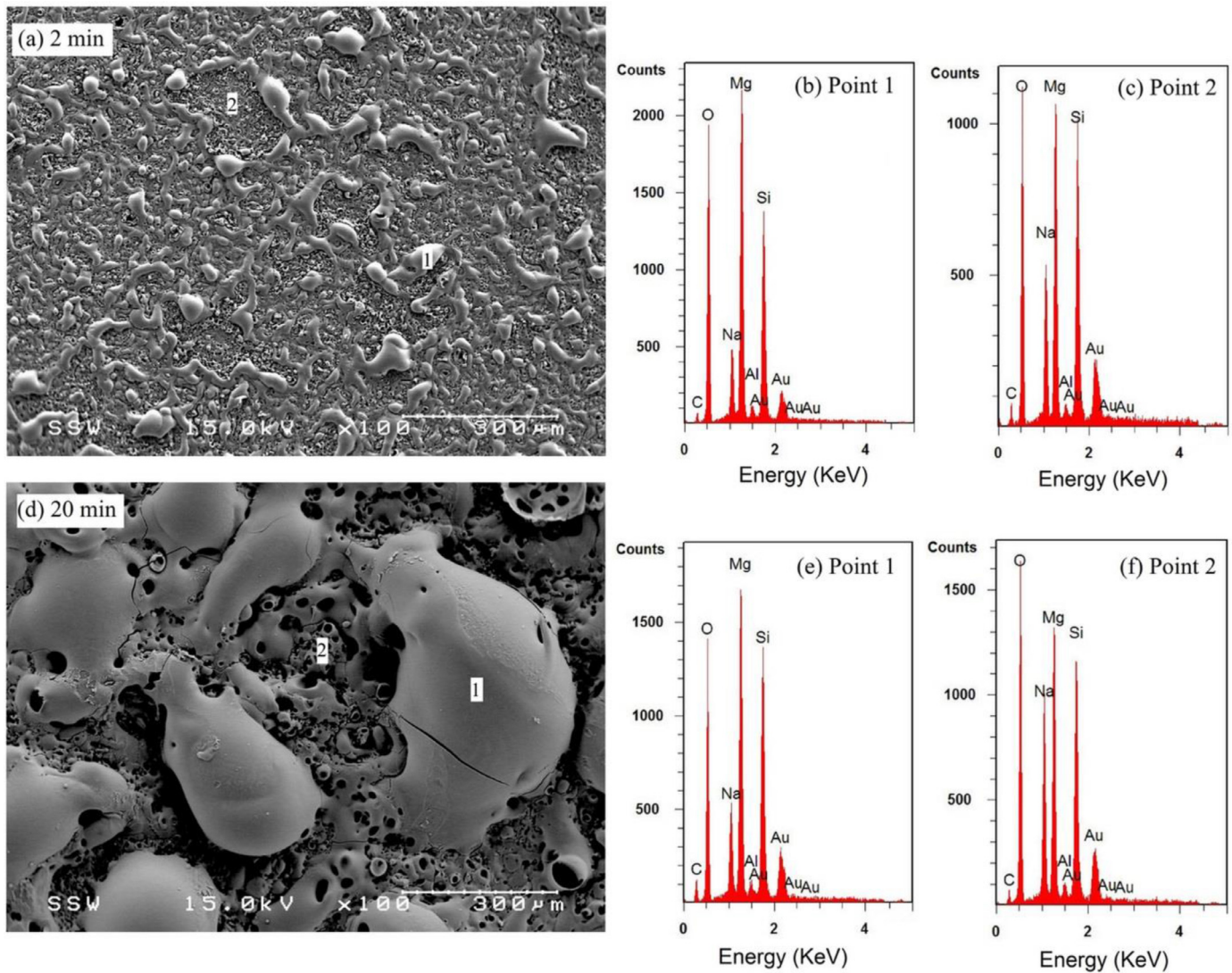


Fig 5. SEM micrographs and EDX spectra for point analyses spectra recorded on the globular features and coating matrix formed on AM50 Mg samples coated for 2 min, (a–c) and 20 min (d–f).

porous matrix was formed by type A discharges, while the globular features were the result of type C discharges. In the matrix, the Al/Si and Mg/Na ratios are lower than those of the globular features, indicating a greater electrolyte contribution to the composition at these locations.

3.3. Phase composition

Diffraction patterns from the uncoated AM50 Mg substrate and from samples coated for different durations from 2 to 20 min, obtained using glancing angle X-ray diffraction (XRD), are presented in Fig. 6. As the coating time increases, the substrate peaks become smaller, as expected for an increase in coating thickness. This is confirmed by the cross-sectional SEM micrographs in Fig. 3. For the sample coated for 20 min, no substrate peak is observed in the XRD pattern. Inspection of the XRD patterns reveals that the coatings are

composed of an amorphous phase, as indicated by the wide, shallow peak in the 2θ range from 20° to 35° .

Lu et al. [43] also reported coatings comprising a single amorphous phase when prepared in electrolytes containing KOH and high Na_3PO_4 concentrations. However, the use of higher concentrations of KOH resulted in coatings with mixed crystalline and amorphous phases, leading them to suggest that the phase content of the coatings could, to some extent, be controlled by varying the electrolyte composition.

4. Discussion

4.1. General features of coating growth

Our low-energy PEO coatings formed at voltages below 200 V show different characteristics than do the common PEO coatings reported in the literature. A crater-like (pancake-like) morphology, with a central hole, is a common characteristic

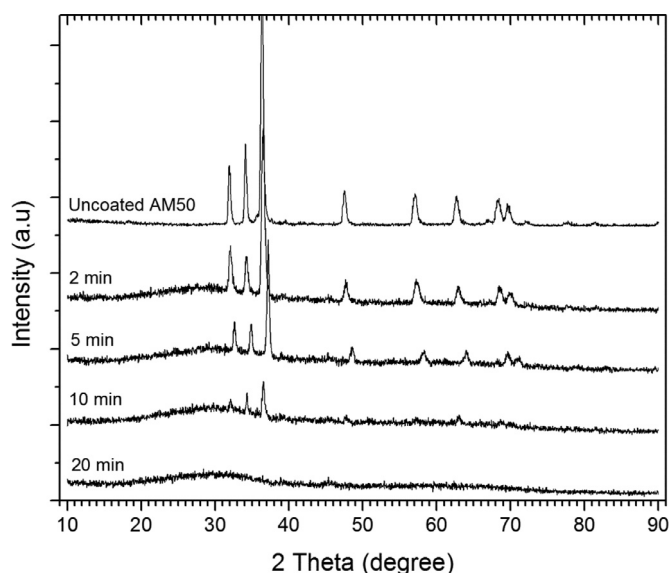


Fig. 6. XRD patterns (glancing angle) of un-coated AM50 Mg and AM50 Mg coated for durations from 2 to 20 min.

of the coatings, and is thought to be caused by strong type B discharges initiating close to the substrate surface. The central holes might penetrate deep into the coating and negatively affect its corrosion properties [44].

The morphology of the coatings, Fig. 2, exhibited two features, a matrix with very small surface pores, and a number of globular features that grew with increasing treatment time to dimensions of a few hundred micrometres after 20 min. A non-uniform coating thickness was observed, with that obtained after 20 min, Fig. 3-f, ranging from 20 μm in the matrix, to 120 μm in the globular structure. The microstructural characteristics and phase composition suggest that the coatings were primarily formed by types A and C discharges. No crater-like morphology, characteristic of type B discharges, was observed, irrespective of the duration of the coating process, Fig 2.

The EDX intensity ratios of Mg/Si and Mg/Na, Table 1, confirm that species from both the substrate and the electrolyte were incorporated into the coatings, which supports their formation by types A and C, and not type B, discharges. Since type B discharges start from the interface between the substrate and the coating, they would result in a much higher concentration of species from the substrate. EDX intensity ratios of Mg/Si and Mg/Na, Table 1, were lower in the porous matrix than in the globular features, irrespective of the duration of the coating process. This suggests that the matrix was most likely formed by type A discharges, while the globular features were the result of type C discharges. Type A discharges occur at the interface of the oxide layer and the electrolyte solution, or in the gases attached to this interface, close to the very small holes in the coating. This leads to the greater incorporation of electrolyte species. By contrast, type C discharges occur deeper within surface defects such as holes or cracks filled with the electrolyte, and result in compositions enriched in substrate elements [37].

4.2. Phase composition

PEO coatings on Mg alloys prepared in electrolyte solutions containing silicates, phosphates and/or aluminates are commonly composed of a combination of amorphous and/or crystalline phases such as MgO, Mg_2SiO_4 , $\text{Mg}_3(\text{PO}_4)_2$, and Mg_2AlO_4 [22,45]. As demonstrated by XRD, the coatings in our study were amorphous. A possibility is that this could be attributed to the local temperatures during the coating process. Plasma electron temperatures have been shown to depend strongly on the type of discharge. Temperature profiles measured by optical emission spectroscopy during PEO on AM60B Mg alloy showed that the baseline average plasma electron temperature ranged from 5500 to 6500 K, depending on the current mode employed. In addition, the profiles contained many closely-spaced temperature spikes, with some reaching 7500 K. These spikes were attributed to strong type B micro-discharges [37,44], suggesting that type B micro-discharges are stronger and, hence, create higher plasma temperatures than types A and C.

This suggests that the possible reason for the dominance of an amorphous phase in our coatings is the predominance of types A and C discharges and the absence of type B discharges. During PEO coating, the molten material created by the discharges solidifies rapidly upon contact with the electrolyte, with faster cooling rates generally promoting the formation of amorphous phases. Types A and C micro-discharges occur at the coating/electrolyte interface, leading to the rapid quenching of the molten material by the electrolyte solution, whereas type B discharges, which originate at the metal-oxide interface, are strong and generate higher temperatures. The higher temperatures generated by type B discharges can enhance amorphous to crystalline phase transformation possibly by two mechanisms. The excess heat can provide the energy required for phase transformation in the amorphous, solid regions surrounding discharge channels and/or it can decrease the cooling rate of the molten material in discharge channels, facilitating its crystallisation. Since our coatings were created mainly by rapidly quenched types A and C discharges, the phases remained amorphous in the absence of type B micro-discharges.

These conclusions are supported by previous observations [46] employing glancing angle XRD to study the phase composition as a function of depth into the coating on an Al alloy. This study showed that the outer surfaces of the coatings were amorphous, with crystalline phases detected as the coating was analyzed at different depths. Arrabal et al. [22], identified MgO and Mg_2SiO_4 as the main components of AC PEO coatings on different Mg alloys in an electrolyte solution containing Na_2SiO_3 and $\text{Na}_4\text{P}_2\text{O}_7 \cdot 10\text{H}_2\text{O}$. Their EDX analyses showed the concentrations of Si and P, coming from the electrolyte, were higher in the outer layers of the coatings, most probably as a consequence of types A and C discharges.

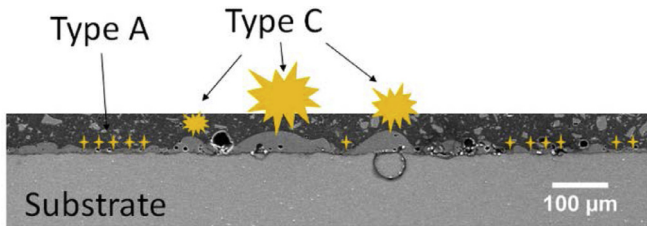


Fig. 7. Schematic representation of a PEO-coated AM50 Mg alloy. The small icons show the thin coating matrix formed by type A discharges. The larger icons show the globular structures associated with type C discharges.

4.3. Voltage-time behaviour

The voltage oscillations starting after ~ 2 min, and persisting thereafter, Fig. 1, are not commonly observed during PEO. Ono et al. [19] and Yagi et al. [36] reported oscillations during PEO treatment of different Mg alloys, but did not offer any explanation. In both studies, concentrated electrolytes were used, but with Na_3PO_4 rather than $\text{Na}_2\text{B}_4\text{O}_7$. These voltage oscillations appear to be caused by the micro-discharges created during PEO treatment. As discussed above, in this study the coatings were primarily formed by types A and C discharges. The porous matrix, with many fine pores, each corresponding to a single discharge, was formed by type A discharges while the globular features, whose number decreased while their size increased with coating time, were the result of type C discharges. Examination of the voltage-time plot in Fig. 1 and the SEM micrographs in Fig. 2, showed no significant oscillations after 1 min of coating and no distinguishable globular features in the SEM micrograph, Fig. 2-a. Once oscillations started after ~ 1.5 min, globular features became easily observable on the sample surfaces, Fig. 2-b to 2-f. The cross-sectional micrographs, Fig. 3, show lateral variations in coating thickness, with the coating formed after 20 min, Fig. 3-f, having a thickness ranging from $20\ \mu\text{m}$ in the matrix, to $120\ \mu\text{m}$ in the globular structure. To create these large structures, the type C discharges must have been stronger than the type A discharges. The voltage-time plot reflects the electric field within the coating [19].

Fig. 7 shows a short cross-section of the coating produced after 3 min. The thinly-coated areas on the surface, marked with small icons, show the location of the coating matrix formed by type A discharges. The three locations where the coating is thicker, marked by larger icons, are likely formed by type C discharges, with the size of the associated icon indicating the intensity of the type C discharges. Since they have higher intensities compared to type A discharges, and initiate deep within surface defects such as holes and cracks, the coating is breached and a large molten mass is ejected, leading to a drop in voltage. The rapid solidification of this molten mass on contact with the electrolyte at the coating/electrolyte interface leads to the formation of the globular structures. This is accompanied by an increase in coating resistance, which would account for the accompanying voltage increase. The voltage oscillations then accompany the repetitive occurrence

of such events. That these fluctuations are superimposed on a steady-state voltage between 100 and 200 V can then be attributed to the fact that the coating formation mechanism does not subsequently change during the coating process, except that these strong discharges progress gradually from a large population of small and frequent micro-discharges towards a smaller population of larger and longer-lasting discharge events. This was confirmed by visual observations during the coating process and the SEM micrographs showing the development of PEO coatings, presented in Fig. 2.

The results presented here suggest electrolyte chemistry can somewhat control discharge behaviour, which plays an important role in PEO coating growth. Coatings obtained in a concentrated electrolyte containing sodium tetraborate in this study, exhibit characteristics of types A and C discharges, as discussed previously, while in studies where electrolytes with different chemical compositions and generally lower concentrations were used, such as 7 g/L $\text{K}_4\text{P}_2\text{O}_7$, 3 g/L $\text{Na}_2\text{Al}_2\text{O}_4$, and 1 g/L KOH [44], 10 g/L Na_2SiO_3 and 10 g/L KOH [47], 15 g/L Na_2SiO_3 and 2 g/L KOH [48], PEO coatings exhibited characteristics of mainly type B discharges.

5. Conclusions

- Low-energy PEO coatings were successfully formed on an AM50 Mg alloy at voltages below 200 V in a concentrated electrolyte solution. Correlations were observed between the voltage-time behaviour, the micro-discharge characteristics and the composition and microstructure of the coated alloy.
- The surface morphology and voltage-time behaviour of coatings were different from those commonly reported for coatings. Instead of the commonly observed crater-like features, the coatings were composed of two features: (i) a matrix with very small surface pores; and (ii) larger globular features. Large voltage oscillations (~ 100 V) were observed during treatment and the coatings formed were amorphous.
- Characterization of the microstructure and analyses of the phase formed indicate that the coatings were primarily formed by types A and C discharges, originating at the coating/electrolyte interface. The porous matrix coating was formed by type A discharges, while the larger globular features were the result of type C discharges. The high cooling rates during the solidification of molten materials produced by these surface discharges resulted in the formation of amorphous phases, which remained amorphous in the absence of type B micro-discharges.
- Voltage oscillations are attributed to the occurrence of type C discharges, which form a large molten mass that decreases the coating resistance leading to a voltage drop. Rapid solidification of this mass then causes an increase in the coating resistance, resulting in a voltage recovery.
- This study suggests that changing the composition of the electrolyte can affect the discharge behaviour, which plays an important role in the growth behaviour of the coating, including thickness and surface morphology.

Acknowledgements

This research was supported by **Natural Science and Engineering Research Council of Canada (NSERC)** grant.

References

- [1] B.V. Vladimirov, B.L. Krit, V.B. Lyudin, N.V. Morozova, A.D. Rossiiskaya, I.V. Suminov, *Surf. Eng. Appl. Electrochem.* 50 (2014) 195–232, doi:10.3103/S1068375514030090.
- [2] Q. Dou, W. Li, G. Zhang, X. Wan, *Mater. Res. Innov* 19 (2015), doi:10.1179/1432891715Z.0000000001309.
- [3] K. Chen, J. Dai, X. Zhang, Improvement of corrosion resistance of magnesium alloys for biomedical applications, *Corros. Rev* 33 (2015) 101–117, doi:10.1515/corrrev-2015-0007.
- [4] G.B. Darband, M. Aliofkhae, P. Hamghalam, N. Valizade, *J. Magnes. Alloy.* 5 (2017) 74–132, doi:10.1016/j.jma.2017.02.004.
- [5] X. Lu, C. Blawert, M.L. Zheludkevich, K.U. Kainer, *Corros. Sci.* 101 (2015) 201–207, doi:10.1016/j.corsci.2015.09.016.
- [6] E. Matykina, R. Arrabal, M. Mohedano, B. Mingo, J. Gonzalez, A. Pardo, et al., *Trans. Nonferrous Met. Soc. China* 27 (2017) 1439–1454, doi:10.1016/S1003-6326(17)60166-3.
- [7] R.O. Hussein, D.O. Northwood, X. Nie, *J. Alloy. Compd.* 541 (2012) 41–48, doi:10.1016/j.jallcom.2012.07.003.
- [8] D. Veys-Renaux, C.-E. Barchiche, E. Rocca, *Surf. Coat. Technol.* 251 (2014) 232–238, doi:10.1016/j.surfcoat.2014.04.031.
- [9] Y. Mori, A. Koshi, J. Liao, H. Asoh, S. Ono, *Corros. Sci.* 88 (2014) 254–262, doi:10.1016/j.corsci.2014.07.038.
- [10] K.C. Tekin, U. Malayoğlu, S. Shrestha, *Surf. Coat. Technol.* 236 (2013) 540–549, doi:10.1016/j.surfcoat.2013.10.051.
- [11] S. Moon, R. Arrabal, E. Matykina, *Mater. Lett.* 161 (2015) 439–441, doi:10.1016/j.matlet.2015.08.149.
- [12] S. Yagi, A. Sengoku, K. Kubota, E. Matsubara, *Corros. Sci.* 57 (2012) 74–80, doi:10.1016/j.corsci.2011.12.032.
- [13] F. Jin, P.K. Chu, G. Xu, J. Zhao, D. Tang, H. Tong, *Mater. Sci. Eng. A* 435436 (2006) 123–126, doi:10.1016/j.msea.2006.07.059.
- [14] K.M. Lee, B.U. Lee, S. Il Yoon, E.S. Lee, B. Yoo, D.H. Shin, *Electrochim. Acta* 67 (2012) 6–11, doi:10.1016/j.electacta.2012.01.053.
- [15] B.H. Ahn, J. Il Song, B.H. Koo, *Trans. Nonferrous Met. Soc. China* 24 (2014) s125–s128, doi:10.1016/S1003-6326(14)63298-2.
- [16] C. Wang, B. Jiang, M. Liu, Y. Ge, *J. Alloys Compd* 621 (2015) 53–61, doi:10.1016/j.jallcom.2014.09.168.
- [17] L. Zhao, C. Cui, Q. Wang, S. Bu, *Corros. Sci.* 52 (2010) 2228–2234, doi:10.1016/j.corsci.2010.03.008.
- [18] D. Sreekanth, N. Rameshbabu, K. Venkateswarlu, C. Subrahmanyam, L. Rama Krishna, K.P. Rao, *Surf. Coat. Technol.* 222 (2013) 31–37, doi:10.1016/j.surfcoat.2013.01.056.
- [19] S. Ono, S. Moronuki, Y. Mori, A. Koshi, J. Liao, H. Asoh, *Electrochim. Acta* 240 (2017) 415–423, doi:10.1016/j.electacta.2017.04.110.
- [20] T.S.N. Sankara Narayanan, I.S. Park, M.H. Lee, *Prog. Mater. Sci.* 60 (2014) 1–71, doi:10.1016/j.pmatsci.2013.08.002.
- [21] R.O. Hussein, X. Nie, D.O. Northwood, *Surf. Coat. Technol.* 205 (2010) 1659–1667, doi:10.1016/j.surfcoat.2010.08.059.
- [22] R. Arrabal, E. Matykina, T. Hashimoto, P. Skeldon, G.E. Thompson, *Surf. Coat. Technol.* 203 (2009) 2207–2220, doi:10.1016/j.surfcoat.2009.02.011.
- [23] Y. Gao, A. Yerokhin, E. Parfenov, A. Matthews, *Electrochim. Acta* 149 (2014) 218–230, doi:10.1016/j.electacta.2014.10.063.
- [24] X. Lu, M. Mohedano, C. Blawert, E. Matykina, R. Arrabal, K.U. Kainer, et al., *Coat. Technol.* 307 (2016) 1165–1182, doi:10.1016/j.surfcoat.2016.08.055.
- [25] F. Monfort, A. Berkani, E. Matykina, P. Skeldon, G.E. Thompson, H. Habazaki, et al., *Corros. Sci* 49 (2007) 672–693, doi:10.1016/j.corsci.2006.05.046.
- [26] C. Liu, D. He, Q. Yan, Z. Huang, P. Liu, D. Li, et al., *Surf. Coat. Technol.* 280 (2015) 86–91, doi:10.1016/j.surfcoat.2015.08.050.
- [27] V. Dehnavi, B.L. Luan, D.W. Shoesmith, X.Y. Liu, S. Rohani, *Surf. Coat. Technol* 226 (2013) 100–107, doi:10.1016/j.surfcoat.2013.03.041.
- [28] W.-C. Gu, G.-H. Lv, H. Chen, G.-L. Chen, W.-R. Feng, G.-L. Zhang, et al., *J. Mater. Process. Technol.* 182 (2007) 28–33, doi:10.1016/j.jmatprotec.2006.07.002.
- [29] Y. Zhang, Y. Wu, D. Chen, R. Wang, D. Li, C. Guo, et al., *Surf. Coat. Technol.* 321 (2017) 236–246, doi:10.1016/j.surfcoat.2017.04.064.
- [30] D. Veys-Renaux, E. Rocca, *J. Solid State Electrochem* 19 (2015) 3121–3129, doi:10.1007/s10008-015-2935-3.
- [31] R. Vasili C, S. Stojadinovi C A, N. Radi C, P. Stefanov, Z. Doh Cevi C-Mitrovi, B. Grbi, One-step preparation and photocatalytic performance of vanadium doped TiO₂ coatings, *Mater. Chem. Phys.* 151 (2015) 337–344, doi:10.1016/j.matchemphys.2014.11.077.
- [32] S. Di, Y. Guo, H. Lv, J. Yu, Z. Li, *Ceram. Int.* 41 (2015) 6178–6186, doi:10.1016/j.ceramint.2014.12.134.
- [33] S. Aliasghari, P. Skeldon, G.E. Thompson, *Appl. Surf. Sci.* 316 (2014) 463–476, doi:10.1016/j.apsusc.2014.08.037.
- [34] A.L. Yerokhin, X. Nie, A. Leyland, A. Matthews, *Surf. Coat. Technol.* 130 (2000) 195–206, doi:10.1016/S0257-8972(00)00719-2.
- [35] E. Matykina, R. Arrabal, P. Skeldon, G.E. Thompson, *Acta Biomater.* 5 (2008) 1356–1366, doi:10.1016/j.actbio.2008.10.007.
- [36] S. Yagi, K. Kuwabara, Y. Fukuta, K. Kubota, E. Matsubara, *Corros. Sci.* 73 (2013) 188–195, doi:10.1016/j.corsci.2013.03.035.
- [37] R.O. Hussein, X. Nie, D.O. Northwood, A. Yerokhin, A. Matthews, *J. Phys. D Appl. Phys.* 43 (2010) 105203–105216, doi:10.1088/0022-3727/43/10/105203.
- [38] Y. Gao, A. Yerokhin, A. Matthews, *Mater. Sci. Eng.* (2015). doi:10.1016/j.msec.2014.12.081.
- [39] H. Li, S. Lu, W. Qin, L. Han, X. Wu, *Acta Astronaut.* 116 (2015) 126–131, doi:10.1016/j.actaastro.2015.07.005.
- [40] R.O. Hussein, D.O. Northwood, X. Nie, *J. Alloy. Compd.* 541 (2012) 41–48, doi:10.1016/j.jallcom.2012.07.003.
- [41] M.M.S. Al Bosta, K.-J. Ma, *Infrared Phys. Technol.* 67 (2014) 63–72, doi:10.1016/j.infrared.2014.07.009.
- [42] B.S. Necula, L.E. Fratila-Apachitei, A. Berkani, I. Apachitei, J. Duszczyc, *J. Mater. Sci. Mater. Med.* 20 (2009) 339–345, doi:10.1007/s10856-008-3589-9.
- [43] X. Lu, S.P. Sah, N. Scharnagl, M. Störmer, M. Starykevich, M. Mohedano, et al., *Surf. Coat. Technol.* 269 (2015) 155–169, doi:10.1016/j.surfcoat.2014.11.027.
- [44] R.O. Hussein, D.O. Northwood, X. Nie, *Mater. Sci. Appl.* 5 (2014) 124–139, doi:10.4236/msa.2014.53017.
- [45] C. Blawert, S.P. Sah, J. Liang, Y. Huang, D. Höche, *Surf. Coat. Technol.* 213 (2012) 48–58, doi:10.1016/j.surfcoat.2012.10.013.
- [46] V. Dehnavi, X.Y. Liu, B.L. Luan, D.W. Shoesmith, S. Rohani, *Surf. Coat. Technol.* 251 (2014) 106–114, doi:10.1016/j.surfcoat.2014.04.010.
- [47] P. Bala Srinivasan, C. Blawert, M. Störmer, W. Dietzel, *Surf. Eng.* 26 (2010) 340–346, doi:10.1179/174329409X379246.
- [48] F. Muhaffel, F. Mert, H. Cimenoglu, D. Höche, M.L. Zheludkevich, C. Blawert, *Surf. Coat. Technol.* 269 (2015) 200–211, doi:10.1016/j.surfcoat.2014.12.057.